Evolution of a neuroprotective function of central nervous system myelin

Xinghua Yin,[1] Rena C. Baek,[2] Daniel A. Kirschner,[2] Alan Peterson,[3] Yasuhisa Fujii,[1] Klaus-Armin Nave,[4] Wendy B. Macklin,[1] and Bruce D. Trapp[1]

[1]Department of Neurosciences, Lerner Research Institute, Cleveland Clinic Foundation, Cleveland, OH 44195
[2]Department of Biology, Boston College, Chestnut Hill, MA 02467
[3]Laboratory of Developmental Biology/Molecular Oncology, McGill University, Montreal, Canada H3A 2T5
[4]Department of Neurogenetics, Max Planck Institute of Experimental Medicine, D-37075 Goettingen, Germany

The central nervous system (CNS) of terrestrial vertebrates underwent a prominent molecular change when a tetraspan membrane protein, myelin proteolipid protein (PLP), replaced the type I integral membrane protein, P_0, as the major protein of myelin. To investigate possible reasons for this molecular switch, we genetically engineered mice to express P_0 instead of PLP in CNS myelin. In the absence of PLP, the ancestral P_0 provided a periodicity to mouse compact CNS myelin that was identical to mouse PNS myelin, where P_0 is the major structural protein today. The PLP–P_0 shift resulted in reduced myelin internode length, degeneration of myelinated axons, severe neurological disability, and a 50% reduction in lifespan. Mice with equal amounts of P_0 and PLP in CNS myelin had a normal lifespan and no axonal degeneration. These data support the hypothesis that the P_0–PLP shift during vertebrate evolution provided a vital neuroprotective function to myelin-forming CNS glia.

Introduction

Myelin is a multilamellar, tightly compacted membrane that surrounds axons in the central nervous system (CNS) and peripheral nervous system (PNS). Myelin helps concentrate voltage-gated Na^+ channels at nodes of Ranvier (Pedraza et al., 2001), the short unmyelinated regions between myelin segments. The nerve impulse jumps from node to node by a process called saltatory conduction, which facilitates rapid nerve communication in an energy-efficient manner. Although mammalian CNS and PNS myelin serve similar functions, they can be distinguished by two major features. First, oligodendrocytes form multiple myelin internodes in the CNS, whereas Schwann cells form single myelin internodes in the PNS. Second, myelin proteolipid protein (PLP), a four-transmembrane-domain protein, represents >50% of the protein in mammalian CNS myelin (Milner et al., 1985), whereas P_0 protein, a type I integral membrane glycoprotein and member of the immunoglobulin gene super family, represents >70% of the total myelin protein in mammalian PNS myelin (Lemke and Axel, 1985).

P_0 was initially the primary structural protein of CNS and PNS myelin, which first appeared ~440 million years ago in cartilaginous fish (Waehneldt et al., 1986; Kirschner et al., 1989; Saavedra et al., 1989; Waehneldt, 1990; Yoshida and Colman, 1996). The DM20 isoform of the *Plp* gene also appeared in cartilaginous fish myelin, where it was apparently coopted by duplication of an ancestral gene (DMα family) that originated in *Drosophila melanogaster* (Stecca et al., 2000) and is expressed today in neurons and epithelial cells (Kitagawa et al., 1993). The PLP protein appeared after the divergence of the bony fish ~400 million years ago (Yoshida and Colman, 1996) and differs from DM20 by the addition of 35 amino acids into exon III (Macklin et al., 1987; Nave et al., 1987). Both PLP and P_0 had high mutational rates until ~300 million years ago. During this period, it is likely that the function of PLP was evolving, with a requirement for the continued coexpression of P_0. However, with the appearance of reptiles/aves, the function of PLP became fully established, allowing the silent dropout of P_0 from CNS myelin (Waehneldt, 1990; Yoshida and Colman, 1996). Once PLP and P_0 expression was separated exclusively into CNS and PNS myelin, their mutation rates dropped dramatically, and both are highly conserved (almost 100%) across all mammalian species analyzed (Kurihara et al., 1997; Hudson, 2004; Kirschner et al., 2004). This suggests an essential role for PLP and/or a detrimental role for P_0 protein in CNS myelin of higher species.

Myelin also provides trophic support, which is essential for axonal survival. Axonal degeneration is the major

Correspondence to Bruce D. Trapp: trappb@ccf.org

Abbreviations used in this paper: APP, amyloid precursor protein; CNP, 2′, 3′-cyclic nucleotide 3′-phoshodiesterase; CNS, central nervous system; MAG, myelin-associated glycoprotein; MBP, myelin basic protein; P, postnatal day; PLP, myelin proteolipid protein; PNS, peripheral nervous system; WT, wild-type.

The Journal of Cell Biology, Vol. 172, No. 3, January 30, 2006 469–478
http://www.jcb.org/cgi/doi/10.1083/jcb.200509174

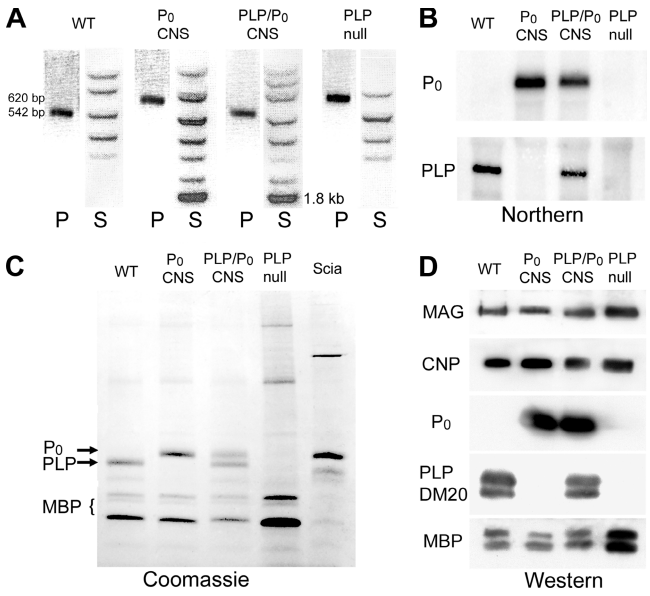

Figure 1. **Replacement of PLP with P_0.** (A) PCR (P) and Southern blot (S) analysis of genomic-tail DNA from WT, P_0-CNS, PLP/P_0-CNS, and PLP-null mice. The diagnostic PCR product for the PLP-null mice was 620 bp in length. The diagnostic band for the P_0 transgene was 1.8 kb. (B) Northern blot analysis of P_0 or PLP mRNA expression in WT, P_0-CNS, PLP/P_0-CNS, and PLP-null mice. P_0 mRNA is present in P_0-CNS and PLP/P_0-CNS; PLP mRNA is present in WT and PLP/P_0-CNS. Neither mRNA is detected in PLP-null CNS. (C) Polyacrylamide gel electrophoresis analysis of myelin proteins from WT, P_0-CNS, PLP/P_0-CNS, and PLP-null mice and WT sciatic nerve. Equivalent amounts of P_0 and PLP are present in myelin isolated from PLP/P_0-CNS mice. Note the presence of P_0 and the absence of PLP in myelin from P_0-CNS mice. (D) Western blot of myelin fractions from WT, P_0-CNS, PLP/P_0-CNS, and PLP-null mice. P_0 protein is present in PLP/P_0-CNS and P_0-CNS myelin; PLP is detected in WT and PLP/P_0-CNS myelin. The genetic manipulations had little effect on levels of MAG, CNP, or MBP.

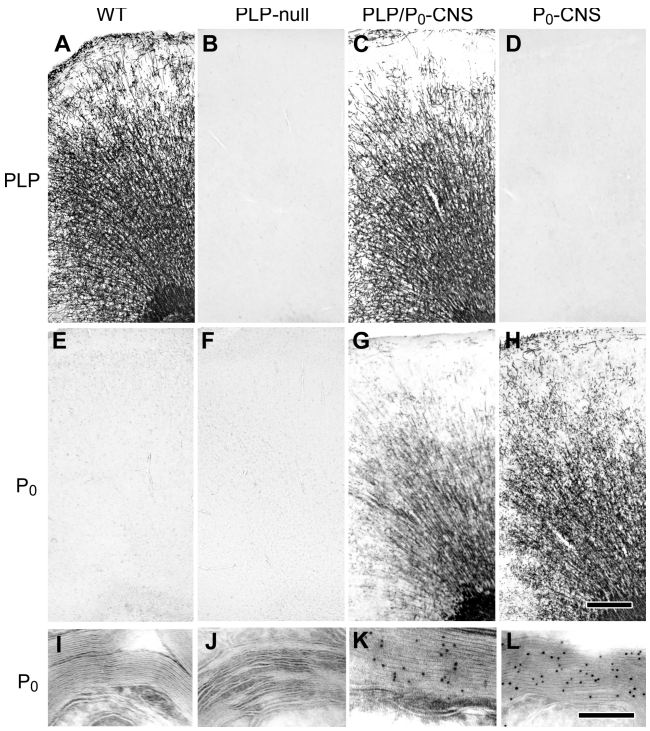

Figure 2. **CNS distribution of PLP and P_0 protein.** (A–D) PLP protein was detected immunocytochemically in WT (A) and PLP/P_0-CNS (C) CNS but not in PLP-null (B) and P_0-CNS (D) CNS. P_0 protein was detected in PLP/P_0-CNS (G) and P_0-CNS (H) CNS but not in WT (E) or PLP-null (F) CNS. Where present, the general distributions of PLP and P_0 were similar and reflected the overall pattern of myelin distribution in P30 mouse brain. At the ultrastructural level, P_0 was not detected immunocytochemically in WT (I) or PLP-null (J) CNS myelin but was abundant in compact CNS myelin in PLP/P_0-CNS (K) and P_0-CNS (L) mice. Bars: (A–H) 200 μm; (I–L) 200 nm.

cause of neurological disability associated with inherited and acquired diseases of myelin (Scherer, 1999; Trapp et al., 1999).

Although the molecular mechanisms responsible for this trophic support are not well understood, mice with a null mutation in the *Plp* gene have a late-onset axonopathy (Griffiths et al., 1998). It remains to be determined whether this axonopathy results from loss of PLP-related trophic support or from alterations in the periodicity and/or stability of PLP-deficient myelin. In addition, mutation and duplication of the human PLP gene is a major cause of the inherited disease of myelin, Pelizaeus-Merzbacher disease. To investigate the possible benefits for the P_0–PLP evolutionary conversion, we "reversed" that evolutionary step using transgenic mice and introduced P_0 expression in exchange for PLP into the mammalian CNS. In the absence of PLP, P_0 protein conferred a highly regular and compact PNS-like structure to CNS myelin. However, because of degeneration of myelinated axons, the lifespan of these mice (compared with wild-type [WT] or PLP-null mice) was reduced by >50%. Based on these data, reversing a discrete step in vertebrate brain evolution demonstrates that the emergence of a new myelin protein was associated with a vital neuroprotective function of myelin-forming CNS glia.

Results

Generation and molecular characterization of mice

Technically, the preferred strategy for expressing P_0 and removing PLP is a direct knockout and knockin of genes by homologous recombination in ES cells. However, when the full-length cDNA encoding P_0 was placed in-frame into exon 2 of the *Plp* gene, mutant mice expressed very little P_0 mRNA, presumably because of the altered spacing of cis-regulatory elements. Therefore we chose to cross mice carrying a P_0 transgene, strongly expressed in oligodendrocytes, on a *Plp*-null background. We generated transgenic mice in which the mammalian P_0 cDNA was driven by 9.1 Kb of the murine myelin basic protein (MBP) promoter (Forghani et al., 2001). These mice were bred to mice null for PLP (Klugmann et al., 1997). The heterozygous F1 pups were interbred to generate pups that were genotyped for PLP and the P_0 transgene. The resulting pups were genotyped and interbred further, and at the F3 generation, mice were identified to be WT, PLP-null, P_0 homozygous transgenic (PLP/P_0-CNS), and P_0 homozygous transgenic plus PLP-null (P_0-CNS; Fig. 1 A). Two lines of mice homozygous for the P_0 transgene were generated, and neither showed a neurological phenotype. The changes described below in mice homozygous

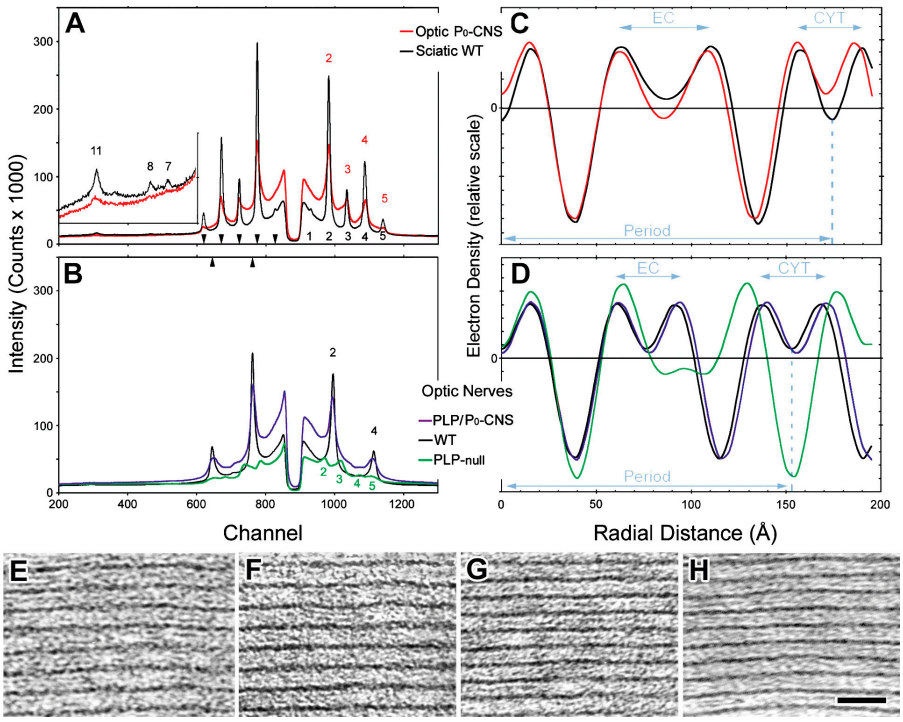

Figure 3. **X-ray diffraction patterns and EM of transgenic and WT compact myelin.** (A) The diffraction pattern of P_0-CNS optic nerve myelin (red) is similar to that of WT sciatic nerve myelin (black) in period (174 Å) and relative intensities of the small-angle region (Bragg orders 1–5) and the wide-angle region (inset, enlarged, with Bragg orders 7, 8, and 11). Note that compared with sciatic, the optic nerve had a smaller peak intensity to background, indicating less myelin. (B) Diffractions from WT optic nerve myelin (black) and optic nerve myelin containing P_0 and PLP (PLP/P_0-CNS; purple) have identical 155-Å periods and relative intensities (Bragg orders 2–4). X-ray scatter from the PLP knockout (PLP-null; green) shows a very weak pattern with expanded arrays of membranes. The positions of the Bragg orders in A and B are marked by the arrowheads. (C and D) Membrane profiles calculated for the diffraction data shown in A and B. Electron density on a relative scale is plotted as a function of radial distance (in angstroms) from the center of a cytoplasmic apposition. There is close correspondence in the intermembrane spaces, measured as the distance between electron-dense peaks, for myelin from P_0-CNS optic nerve and WT sciatic (C) and for optic nerves PLP/P_0-CNS and WT (D). The periodicity and apposition of extracellular (EC) and cytoplasmic (CYT) membrane leaflets is shown for WT myelin from PNS (C) and optic nerve (D). In contrast, PLP-null optic nerve had a much larger extracellular space between membranes and a 194-Å period. In transmission electron micrographs, the periodicity of P_0-CNS myelin (E) is identical to WT PNS myelin (F). The periodicity of PLP/P_0-CNS myelin (G) is identical to WT CNS myelin (H). Bar, 20 nm.

for the P_0 transgene and null for PLP are therefore not caused by insertional mutagenesis.

These four mouse lines were maintained and included in the present study. To determine whether the genotypes translate to the mRNA level, total brain RNA was isolated from all four lines at postnatal day (P) 60 and probed with P_0 and PLP cDNAs by Northern blot (Fig. 1 B). These data establish that the P_0 transgene is abundantly transcribed in the CNS and that mice null for PLP mRNA express significant levels of P_0 mRNA.

Myelin was also prepared from P60 brains, and its protein composition was analyzed on SDS gels (Fig. 1 C). As expected, WT CNS myelin contained PLP, myelin from PLP/P_0-CNS mice contained P_0 and PLP, P_0-CNS myelin contained P_0, and PLP-null mice contained neither P_0 nor PLP. The levels of P_0 and PLP were similar in the PLP/P_0-CNS myelin, and the level of P_0 in the P_0-CNS myelin appeared similar to PLP in WT myelin. Our goal of replacing PLP with similar levels of P_0 was therefore achieved. We also compared levels of three other myelin proteins, myelin-associated glycoprotein (MAG), 2′, 3′-cyclic nucleotide 3′-phoshodiesterase (CNP), and MBP in CNS myelin purified from the four lines of mice by Western blot (Fig. 1 D). There were no significant differences in levels of these myelin proteins except their increase in PLP-null myelin, which reflects their relative contribution to total myelin proteins after the loss of PLP, i.e., 50% of the total myelin protein.

We next determined the cellular distribution of P_0 and PLP in the different mice by immunocytochemistry (Fig. 2). P_0 protein was synthesized by oligodendrocytes in P_0-CNS and PLP/P_0-CNS mice and targeted to myelin internodes. At the light microscopic level, the distribution of P_0 (Fig. 2, G and H) was indistinguishable from PLP in WT (Fig. 2 A) or PLP/P_0-CNS (Fig. 2 C) brains. To determine whether P_0 was targeted to compact myelin, we performed electron microscopic immunocytochemistry using immunogold procedures (Fig. 2, I–L). P_0 was not detected in compact myelin from WT (Fig. 2 I) or PLP-null (Fig. 2 J) mice but was abundant in PLP/P_0-CNS (Fig. 2 K) and P_0-CNS (Fig. 2 L) compact myelin. When expressed, P_0 protein did not accumulate in mouse oligodendrocyte perinuclear cytoplasm, nor was it targeted to paranodal loops or oligodendrocyte plasma membranes. Similar to their amphibian ancestors, mammalian oligodendrocytes maintain their ability to appropriately and exclusively target P_0 to compact myelin.

P_0 stabilizes compact CNS myelin

To investigate the possible impact of P_0 protein on the periodicity or membrane spacing of CNS myelin, we analyzed optic nerves from the mice by x-ray diffraction and transmission EM. X-ray diffraction measures myelin periodicity and membrane packing of unfixed, freshly dissected nerves. As documented previously (Schmitt et al., 1941), typical CNS and PNS myelin diffraction patterns are readily distinguished from one another by the spacing between reflections (which signals the periodicity) and by the number of reflections. Thus, for WT animals, CNS myelin shows two strong Bragg orders (the second and fourth) from an ~155-Å periodicity, whereas PNS myelin shows four distinctive Bragg orders (the second through fifth) from an ~174-Å periodicity (Kirschner and Blaurock, 1992).

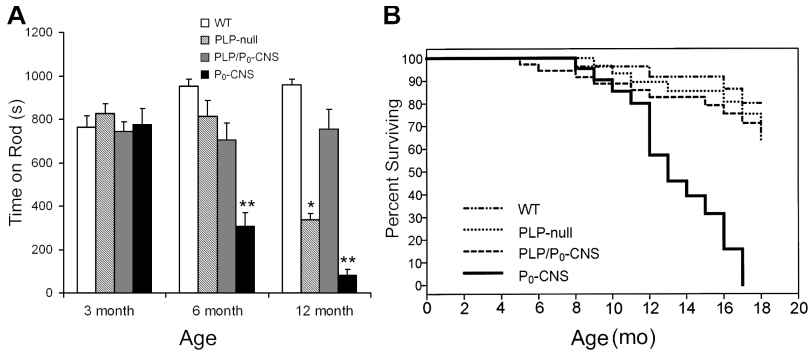

Figure 4. **Reduced motor performance and increased mortality in P_0-CNS mice.** (A) Analysis of standard rota-rod test of mice at 3, 6, and 12 mo of age. Rota-rod performance was similar for all four strains of mice at 3 mo of age. At 6 mo of age, motor performance was significantly reduced in P_0-CNS mice and similar in the other lines. At 12 mo of age, performance of P_0-CNS mice worsened and performance of PLP-null mice was significantly reduced when compared with WT and PLP/P_0-CNS mice (*, $P < 0.0001$; **, $P < 0.001$). (B) Kaplan-Meier curve assessing survival as a function of age for the four lines of mice. The mean lifespan of P_0-CNS mice was reduced by 50% compared with the other lines of mice, which had mortality rates similar to those of WT (n = 30 WT, 40 PLP-null, 40 PLP/P_0-CNS, and 30 P_0-CNS mice).

Optic nerves from P_0-CNS mice gave a diffraction pattern that was identical to WT sciatic nerve; i.e., the positions of the reflections and the relative intensities were the same (Fig. 3 A). This was true even for the higher resolution region of the patterns, where higher Bragg orders were detected (Fig. 3 A, inset). The membrane profiles (Fig. 3 C) that were calculated from the diffraction data showed similar dimensions: as measured from the positions of the centers of the electron-dense peaks, the membrane bilayers were ~47 Å wide, the cytoplasmic appositions were ~32 Å wide, and the extracellular spaces were ~48 Å wide. The only significant difference between the myelin diffraction from WT sciatic and P_0-CNS optic nerves was the overall stronger intensity of the WT sciatic nerve. This difference reflects thicker myelin internodes (more lamellae) in the PNS than in the CNS.

For optic nerves from PLP/P_0-CNS mice, the diffraction patterns were virtually identical to WT CNS myelin (Fig. 3 B), i.e., with the second and fourth Bragg orders being the strongest and located at positions corresponding to a 155-Å periodicity. The membrane profiles calculated from these patterns showed similar dimensions, with ~47-Å-wide bilayers, ~32-Å-wide cytoplasmic spaces, and ~32-Å-wide extracellular spaces (Fig. 3 D). Thus, despite its known homophilic interactions in trans (D'Urso et al., 1990; Filbin et al., 1990), P_0 appeared to have little affect on myelin spacing when expressed at equal amounts with PLP. The x-ray scatter recorded from PLP-null optic nerves (Fig. 3 B) indicated expanded arrays of disordered membranes, with a 194-Å periodicity compared with the 155-Å period of WT optic nerve myelin. Consistent with the diffraction data, electron micrographs showed that the periodicity of compact myelin in P_0-CNS optic nerves (Fig. 3 E) was identical to compact myelin in WT sciatic nerves (Fig. 3 F) and greater than that of compact myelin in WT optic nerves (Fig. 3 G) or PLP/P_0-CNS optic nerves (Fig. 3 H).

Neurological disability and mortality

To determine the effect of replacing PLP with P_0 on motor function, we compared the performance of P_0-CNS mice on a standard rota-rod treadmill with that of WT, PLP/P_0-CNS, or PLP-null mice at 3, 6, and 12 mo of age (Fig. 4 A). At 3 mo of age, all strains of mice performed similarly. At 6 mo of age, the performance of WT, PLP/P_0-CNS, and PLP-null mice was indistinguishable, whereas that of the P_0-CNS mice was reduced by 70%. Compared with WT mice at 12 mo of age, the performance of P_0-CNS and PLP-null mice was reduced by 90 and 60%, respectively, whereas the performance of PLP/P_0-CNS mice was unchanged. We terminated these experiments at 12 mo of age because of the high mortality rate of the P_0-CNS mice.

The mortality rate of P_0-CNS mice was compared with that of WT, PLP/P_0-CNS, and PLP-null mice (Fig. 4 B). There was no difference in the mortality rate of WT, PLP/P_0-CNS, and PLP-null mice. The mortality rate of P_0-CNS mice, however, was significantly increased. Approximately 50% of the P_0-CNS mice died by 12 mo of age. 80% were dead by 16 mo, and none lived past 18 mo, when 70% of the other strains were still surviving. Thus, replacing PLP with P_0 in mouse CNS myelin causes the premature death of these mice.

Axonal pathology and degeneration

The reduced lifespan of P_0-CNS mice and the earlier demonstration of axonal pathology in PLP-null mice (Griffiths et al., 1998) prompted histological examination of the P_0-CNS mice for underlying neurodegenerative changes. We performed a detailed analysis of the amyloid precursor protein (APP) in the brains from the four lines of mice. APP detection is a reliable indicator of axonal pathology in primary myelin disease affecting PLP-null mice (Griffiths et al., 1998; Edgar et al., 2004) and humans with multiple sclerosis (Ferguson et al., 1997). APP is only detected in axons with compromised axonal transport (Koo et al., 1990). A dramatic increase in APP immunoreactivity occurred in the P_0-CNS brains compared with the brains from the other three lines (Figs. 5, A–D). This APP immunoreactivity appeared predominately as small ovoids. This is consistent with previous identification of APP accumulation in axonal swellings (Griffiths et al., 1998; Edgar et al., 2004). We quantified APP-positive ovoid densities in the cerebral cortex from 1-, 3-, 6-, and 12-mo-old mice. WT (Fig. 5 A) and PLP/P_0-CNS (Fig. 5 C) mice contained few APP-positive swellings. In contrast,

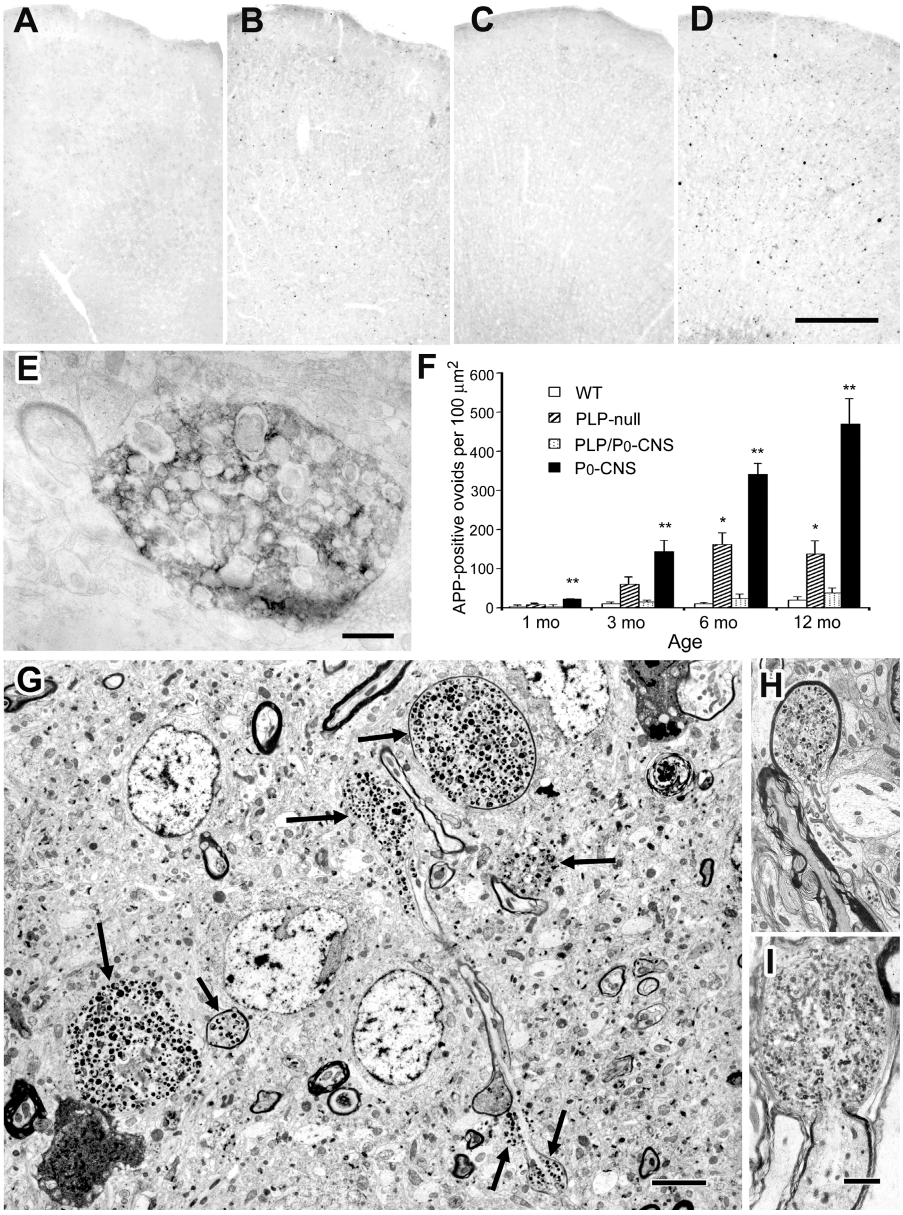

Figure 5. **Axonal pathology and APP accumulation in P_0-CNS mice.** (A–D) Cerebral cortex sections from 12-mo-old WT (A), PLP-null (B), PLP/P_0-CNS (C), and P_0-CNS (D) mice stained with APP antibodies. APP-positive ovoids are prominent in P_0-CNS and present in PLP-null sections. (E) Electron microscopic immunocytochemistry identified these APP-positive ovoids as swollen axons. (F) Quantification of APP ovoid density at 1, 3, 6, and 12 mo of age. At 3 mo, APP ovoids were present in P_0-CNS mice but not in the other lines of mice. APP-positive ovoids progressively increased at 3, 6, and 12 mo of age in P_0-CNS sections and remained at low levels in WT and PLP/P_0-CNS sections. APP-positive ovoids in PLP-null mice were detected at 3 mo of age and increased at 6 mo of age but were significantly less than those in P_0-CNS mice. (G–I) Ultrastructure of axonal swellings in 12-mo P_0-CNS cerebral cortex. Organelle-filled axonal swellings occurred throughout the cerebral cortex of P_0-CNS mice (G, arrows). When viewed in longitudinal orientation (H and I), most swellings were located at distal paranodes. Data was analyzed by a *t* test. Each bar in F represents data from nine sections (three sections from three mice; *, $P < 0.05$; **, $P < 0.01$). Bars: (A–D) 200 µm; (E) 0.25 µm; (G) 5 µm; (H and I) 2.5 µm.

APP swellings were abundant in the cortices from the P_0-CNS (Fig. 5 D) and PLP-null (Fig. 5 B) mice. The density of these swellings was greater in P_0-CNS cortices than in PLP-null cortices and thus correlated with the more severe neurological phenotype and reduced lifespan. A small but statistically significant increase in APP swellings was detected in P30 P_0-CNS cortices when compared with the other three lines. Compared with PLP-null cortices, P_0-CNS cortices contained approximately twice the number of axonal swellings at 3 and 6 mo of age and over three times the number at 1 yr.

We confirmed the identification of APP-positive ovoids as myelinated axonal swellings using postembedding electron microscopic immunocytochemistry (Fig. 5 E). Transmission EM detected a dramatic increase in the number of organelle-filled axonal swellings in the cerebral cortex from 1-yr-old P_0-CNS cortices (Figs. 5, G–I). As described in PLP-null mice (Griffiths et al., 1998; Edgar et al., 2004), APP-positive swellings occurred predominantly at distal paranodes. To determine whether axonal pathology occurred throughout the neural axis in P_0-CNS mice, we quantified axonal swellings and axonal degeneration in the dorsal cervical spinal cord (corticospinal tracts) at 6 mo of age (Fig. 6). Myelinated axonal pathology was not detected in WT and PLP/P_0-CNS dorsal columns (not depicted) but was present in PLP-null (Fig. 6 A) and P_0-CNS (Fig. 6 B) dorsal columns. The density of swollen axons and myelinated axons undergoing Wallerian degeneration (Fig. 6 C) was three times greater in P_0-CNS than in PLP-null mice. These and data not shown detected axon ovoids in the optic nerves, diencephalons, and brain stems of P_0-CNS mice.

The data described in the previous paragraph indicate that replacement of PLP by P_0 either accelerates the formation paranodal axonal ovoids or increases the number of axonal ovoids formed. Because axonal ovoids occur at paranodal regions, we investigated whether P_0-CNS mice have greater

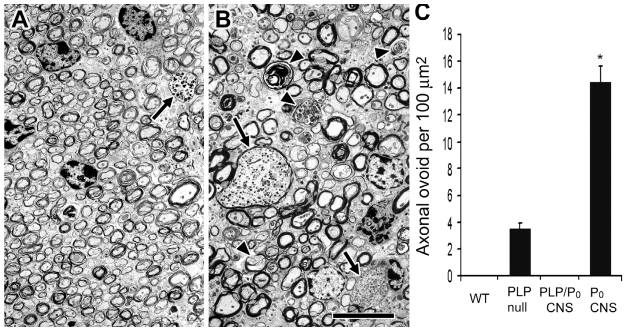

Figure 6. **Myelinated axonal pathology in P_0-CNS cervical spinal cord.** (A and B) Axonal swellings (arrows) and degenerating internodes (arrowheads) were identified in electron micrographs of the cortical spinal tract of 6-mo-old PLP-null (A) and P_0-CNS (B) mice. (C) Axonal pathology was five times more abundant in P_0-CNS than in PLP-null mice. Error bars represent SEM. *, $P < 0.001$. Bar, 100 µm.

nodal densities than WT and PLP-null mice. Sections from month-old P_0-CNS and WT optic nerves were double labeled with antibodies specific for Na^+ channels and caspr, molecules enriched in nodal and paranodal axolemma, respectively (Einheber et al., 1997; Arroyo et al., 1999; Rasband et al., 1999). As described previously (Rasband et al., 1999), Na^+ channels were clustered between caspr-positive paranodal regions in WT and P_0-CNS sections (Figs. 7, A and B). Quantification of Na^+ channel cluster density detected a 50% increase in nodes of Ranvier in the P_0-CNS optic nerves (Fig. 7 C). This interpretation was confirmed by electron microscopic examination of optic nerve sections. Nodes of Ranvier were rarely detected in electron micrographs of WT optic nerves, consistent with long internodal lengths. In contrast, it was common to view short internodes in P_0-CNS optic nerve (Fig. 7, D and E). In addition, axon organelles had begun to accumulate at distal paranodes and form intra-axonal ovoids (Fig. 7 E). Nodal density was increased twofold in P_0-CNS optic nerves when compared with WT nerves. Because a previous study (Edgar et al., 2004) reported similar internodal distances in PLP-null and WT mice, these observations establish that replacement of PLP with P_0 induces a gain-of-function mutation that inhibits longitudinal growth of internodal CNS myelin. This generates more paranodes, which cause more axonal pathology, severe neurological deficits, and early death. Although short internodes can result from demyelination/remyelination, we saw no evidence of macrophage-mediated myelin stripping or asymmetric internodal lengths suggestive of segmental demyelination/remyelination. Some fibers were undergoing Wallerian degeneration, in which myelin breakdown is secondary to axonal degeneration.

Discussion

The purpose of this study was to investigate whether the shift from P_0 to PLP during CNS myelin evolution was related to a new function of myelinating CNS glia. After genetic reversal of this shift in mice, we conclude that PLP expression in mammalian oligodendrocytes and/or CNS compact myelin has a neuroprotective benefit for axons. This conclusion is based on the severe neurological deficits, significant axonal degeneration, and dramatically reduced lifespans of mice whose oligodendrocytes express P_0 instead of PLP. Mice expressing both PLP and P_0 in CNS myelin had normal lifespans and no neurological disability or axonal degeneration. Therefore, the mere presence of P_0 in CNS myelin does not appear to be responsible for the phenotypes in P_0-CNS mice. These data suggest that mammalian CNS myelination sets up an axonal dependency on glial trophic signals that requires PLP and that cannot be replaced by reintroduction of the ancestral CNS myelin protein P_0.

P_0 and PLP family members coevolved with myelinating cells in the CNS of fish where P_0 mediates membrane adhesion of compact myelin (Kirschner et al., 1989; Saavedra et al., 1989). The earliest PLP family members are in fact more closely related to the alternatively spliced DM20 isoform of mammalian PLP. PLP/DM20 evolved and coexisted with P_0 in amphibian compact CNS myelin (Yoshida and Colman, 1996). The positively charged 35–amino acid sequence that distinguishes PLP from DM20 (Nave et al., 1987) has been proposed to play an important role in stabilizing myelin membrane compaction and to permit the phenotypically silent dropout of P_0 from terrestrial vertebrate CNS myelin (Yoshida and Colman, 1996). We propose an alternate and/or additional hypothesis that highlights a CNS axon trophic role for PLP established during oligodendrocyte evolution. A role for PLP in maintaining the integrity and long-term survival of mammalian CNS axons was proposed previously, based on axon ovoids and axonal degeneration in the CNS of PLP-null mice (Griffiths et al., 1998). In those studies, however, it was impossible to determine whether the axonal degeneration was a primary effect of PLP loss or a secondary response caused by alterations in the periodicity and/or stability of PLP-deficient myelin. This issue is resolved in the current study, where the neuroprotective effect of PLP was uncoupled from its role in CNS myelin compaction by stabilizing compact CNS myelin with P_0 protein.

Our Western blot analysis of myelin fractions isolated from transgenic and control mice indicated that total amounts of P_0 and/or PLP were similar in P_0-CNS, PLP/P_0-CNS, and WT mice. When expressed with or without PLP, P_0 was appropriately targeted to compact myelin. When overexpressed in oligodendrocytes, PLP becomes toxic and eventually kills the oligodendrocyte (Kagawa et al., 1994; Readhead et al., 1994). When overexpressed in Schwann cells, P_0 is mistargeted to Schwann cell surface membranes and inhibits the spiral wrapping of myelin, which causes amyelination and severe neurological disability (Wrabetz et al., 2000; Yin et al., 2000). The axon ovoids described here in P_0-CNS mice are not present in either P_0- or PLP-overexpressing mice. In addition, oligodendrocyte death and amyelination did not occur in P_0-CNS or PLP/P_0-CNS mice. The phenotypes and pathologies of P_0-CNS mice result from changes in myelin protein composition and not from increased myelin protein dosage.

The periodicity of compact CNS and PNS myelin differs, and each reflects molecular features of PLP and P_0, respectively (Trapp and Kidd, 2004). The extracellular domain of P_0 is larger than that of PLP, and thus the space between the extracellular leaflets and overall periodicity of PNS myelin are each ~20 Å greater than that found in CNS myelin. Our immunocytochemical

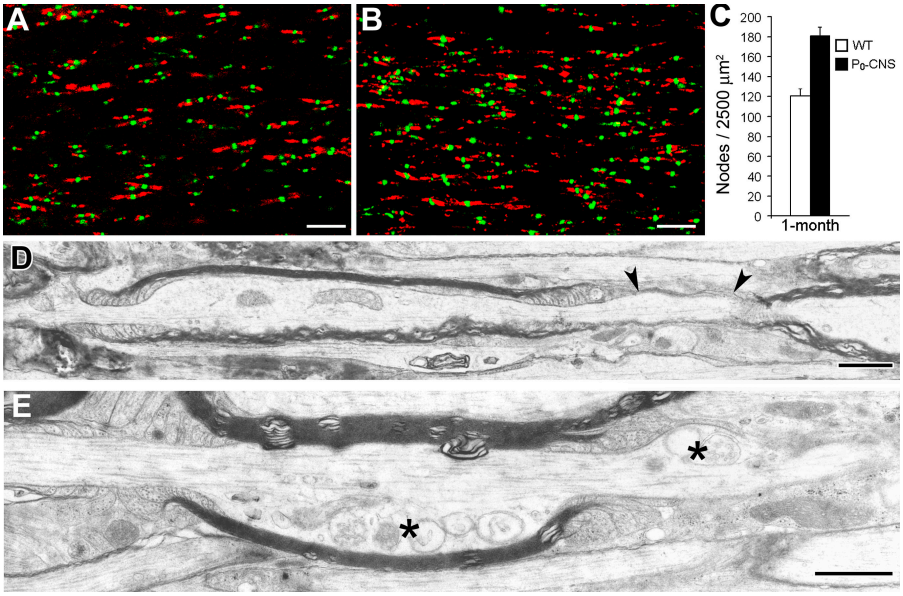

Figure 7. **Nodal density is increased in P_0-CNS optic nerves.** Confocal microscopy of optic nerve sections from WT (A) and P_0-CNS (B) mice stained for Na^+ channels (green) and caspr (red) to mark nodal and paranodal regions, respectively. When quantified, there was an ~50% increase in number of nodes detected in P_0-CNS nerves per confocal field (C; field dimensions 50 × 50 × 6 µm). By EM, P_0-CNS optic nerve axons exhibited very short, thin internodes (D and E), with some ending in elongated nodes (between arrowheads in D). Abnormal intra-axonal organelle accumulations were also observed (E, asterisks). Error bars represent SEM. Bars: (A and B) 10 µm; (D and E) 2 µm.

and Western blot studies demonstrate that when expressed by oligodendrocytes, P_0 protein is targeted to CNS myelin. When P_0 and PLP coexist in compact mouse CNS myelin, they have the periodicity of CNS myelin (Fig. 3). This was unexpected, as one might predict that obligate P_0 homophilic adhesions (Filbin et al., 1990; D'Urso et al., 1990) would dominate putative weaker electrostatic trans-binding of PLP to charged lipids (Trapp and Kidd, 2004). Because P_0 homophilic adhesion may occur by trans-binding between cis-linked P_0 tetramers (Shapiro et al., 1996), it is possible that PLP interferes with P_0 tetramer formation in cis. P_0 monomers or dimers would have little effect on the periodicity of myelin because they cannot bind in trans. In contrast, in the absence of PLP, P_0 tetramers would form and bind in trans, thus dominating the spacing of compact CNS myelin, giving it the periodicity of PNS myelin, as seen ultrastructurally and when examined by x-ray diffraction (Fig. 3). Lipid bilayer thickness and cytoplasmic spacing of CNS and PNS myelin are identical and were unchanged in P_0-CNS and PLP/P_0 optic nerves. P_0, therefore, can replace but not compete with PLP as the major structural protein of CNS mammalian myelin. These observations support the concept that PLP evolved to serve functions unrelated to compact myelin formation.

How does PLP maintain axonal integrity? Although it remains to be determined whether PLP plays a direct or indirect role, observations from the PLP-null and P_0-CNS mice provide clues to biological mechanisms. PLP-null mice have reduced anterograde and retrograde axonal transport that manifest as organelle accumulations at nodes of Ranvier (Griffiths et al., 1998; Edgar et al., 2004). Mice chimeric for the X-linked PLP-null allele (50% of myelin internodes lack PLP) have numerically 50% of the axonal ovoids present in PLP-null mice (Edgar et al., 2004). This implies that PLP facilitates paranodal axonal cytoskeletal organization at the level of individual myelin internodes. Unraveling the precise mechanism by which PLP provides tropic support to the axon presents a significant challenge as the axonopathy evolves over several months and is likely to involve altered molecular complexes that organize the axon cytoskeleton in paranodal regions of myelinated fibers. Based on the chimeric mouse data cited above, a generalized axonal defect or altered neuronal gene expression seem unlikely causes of initial axonal pathology in PLP-null mice. This issue is further complicated as a null mutation in another myelin-specific protein, CNP, which produces axon ovoids similar in appearance to those in PLP-null mice. Like the P_0-CNS mice, CNP-null mice have earlier and more extensive axonal pathology, decreased motor performance at earlier ages, and reduced life spans (Lappe-Siefke et al., 2003). Some CNP-null mice have enlarged ventricles (Lappe-Siefke et al., 2003), a feature not present in P_0-CNS or PLP-null mice. Whether hydrocephalus contributes to or results from axonal loss in CNP-null mice remains to be determined. Ovoids are not the only myelin-induced axonal pathology, as axonal atrophy occurs in MAG-deficient mice (Yin et al., 1998). These changes also have late onset (after 6 mo), manifest in paranodal axoplasm, and include reduced phosphorylation and spacing of neurofilaments (Yin et al., 1998).

Because P_0-CNS mice have more axonal pathology than PLP-null mice, the PLP–P_0 shift in CNS myelin causes a gain-of-function mutation that accelerates and/or increases focal reductions in axonal transport caused by PLP loss of function. Immunocytochemical and electron microscopic examination of myelin internode length in optic nerves established that P_0-CNS mice have shorter myelin internodes, resulting in a greater density of paranodal specializations, which increased and accelerated alterations in axonal transport, formation of axonal ovoids, axonal degeneration, and neurological disability.

The addition of the positively charged 35–amino acid sequence that distinguishes PLP from DM20 (Nave et al., 1987) may play a crucial role in axonal trophic support, as DM20 was unable to rescue the late-onset axonopathy in PLP-null mice (Stecca et al., 2000). Furthermore, it is possible that this 35–amino acid sequence evolved solely for this function, as this PLP-specific sequence shows no significant homology with any other mammalian protein. The data presented here have important implications for human diseases of myelin, as a spectrum of

neurological disabilities is associated with null mutations, duplications, and various point mutations in the PLP gene (Seitelberger, 1995; Hodes and Dlouhy, 1996). Recent studies have reported axonal degeneration in individuals with PLP deletions or point mutations (Garbern et al., 2002). Genotype–phenotype correlations focusing on axonal degeneration and point mutations may identify specific regions of PLP that mediate axonal survival in the human CNS. Such information may lead to the development of novel neuroprotective therapies in inherited and acquired diseases of CNS myelin, such as Pelizaeus-Merzbacher disease and multiple sclerosis.

Materials and methods

Generation of P_0 transgenic mice

We generated transgenic mice that expressed the mouse P_0 cDNA (Lemke and Axel, 1985) ligated to a 9.1-kb region of the mouse MBP promoter (Forghani et al., 2001). These mice were maintained in the animal colony as homozygous animals, and they displayed no obvious behavior abnormalities. *Plp*-null mice (Klugmann et al., 1997) were crossed with homozygous mice carrying the MBP-P_0 transgene. These mice were interbred for three generations to obtain mice that were PLP-null and homozygous for the MBP-P_0 transgene (P_0-CNS), as determined by genomic DNA analysis and outbreeding.

Genomic DNA analysis

DNA was prepared from tail clips by standard proteinase K/phenol chloroform extraction (Haney et al., 1999). Samples were analyzed by Southern blot or PCR to track the P_0 transgene and the *Plp* gene, respectively. For Southern blot analysis, 10 μg of tail DNA was digested with EcoRI overnight and then separated on 1% agarose gels. Gels were blotted and then probed with a random primed 1.8-kb P_0 probe (Lemke and Axel, 1985). WT DNA contained four bands, and additional novel bands were found with the P_0 transgene, most prominently a diagnostic 1.8-kb fragment. The PLP-null mutation was analyzed by PCR, which generated a 620-bp fragment from WT DNA and a 542-bp fragment from PLP-null DNA. The PCR program was 94°C × 3 min; 40 cycles of 94°C × 30 s; 55°C × 30 s; 72°C × 30 s; and 72°C × 7 min. The PCR primers used were 5′-ACGAGCAGTGAGAGTTGGGT-3′ and 5′-AGTCTGTTTTGCGGCTGACT-3′.

RNA expression

Total RNA was prepared from P60 brains using the RNAgents total RNA isolation system (Promega). 5-μg samples were separated on 1% agarose gels and probed with P_0 or PLP cDNA as described previously (Trapp et al., 1988; Kidd et al., 1990).

Protein expression

Myelin was prepared from homogenates of P60 brains from WT, PLP-null, PLP/P_0-CNS, and P_0-CNS mice according to established procedures (Norton and Poduslo, 1973). In brief, brains were homogenized in 0.32 M sucrose and myelin was prepared by differential and gradient centrifugation as a fraction that floats on 0.88 M sucrose. This fraction was osmotically shocked and centrifuged. Samples were analyzed on 12% polyacrylamide gels and stained (10 μg of protein) with Coomassie blue or blotted (2 μg of protein) for Western analysis with PLP/DM20 antibody (clone AA3; a gift from S. Pfeiffer, University of Connecticut Health Science Center, Farmington, CT), P_0 antibody (Trapp et al., 1981), MAG antibody (a gift from R. Quarles, National Institutes of Health, Bethesda, MD), CNP, or MBP antibodies (Sternberger Monoclonals).

Motor function and mortality

To access motor function, we used the rota-rod test as described previously (Griffiths et al., 1998). Five mice from each strain were tested at 3, 6, and 12 mo of age. All mice were placed on the roller at the initial speed of 2 rpm. The speed was continuously increased over a period of 5 min to a final rate of 20 rpm. The time each mouse remained on the roller was recorded, and differences between strains were determined by performing a *t* test. A Kaplan-Meier analysis of mortality was conducted for a minimum of 30 mice from each strain.

Immunocytochemistry

WT, PLP-null, PLP/P_0-CNS, and P_0-CNS mice were perfused with 4% paraformaldehyde and 0.08 M Sorenson's phosphate buffer. Brains were removed, immersion fixed overnight, cryoprotected, frozen, and sectioned (30 μm thick) on a sliding microtome. Free-floating sections were treated with PBS containing 3% normal goat serum and 1% Triton X-100 for 1 h at room temperature. Sections were incubated overnight at 4°C with PLP/DM20 antibody (1:100) or P_0 antibody (1:800) in PBS containing 1% normal goat serum/0.01% Triton X-100. Sections were developed with the avidin biotin complex kit (Vector Laboratories) and diaminobenzidine as described previously (Trapp et al., 1997). Sections were photographed in a photomicroscope (Axiophot; Carl Zeiss MicroImaging, Inc.) with standard 2.5–20× dry lenses using a Magnafire (Optronics) digital camera and software. For analysis of APP accumulation, three mice from each strain were processed at 1, 3, 6, and 12 mo of age. Sections were immunostained with APP antibodies (Zymed Laboratories) as described above. The density of APP-positive axonal swellings was quantified in three sections from each mouse at all ages. Differences in APP densities were determined by *t* test. To identify APP-positive structures as axonal swellings, several APP-stained 30-μm sections from P_0-CNS mice were processed for EM as described previously (Trapp and Quarles, 1984). Sections were viewed and photographed in an electron microscope (CM-100; Phillips). Light and electron microscope images were prepared for publication using Photoshop 7.0 software (Adobe).

The distribution of P_0 protein was also determined at the ultrastructural level. P30 mice were perfused with 2.5% glutaraldehyde, 4% paraformaldehyde, and 0.08 M Sorensen's phosphate buffer. The ventral cervical spinal cord was removed and infiltrated with 30% polyvinlpyrolidine and 2.3 M sucrose. The tissue was cut in a Ultracut S ultracryomicrotome (Reichert) maintained at −110°C. Sections were placed on carbon- and formvar-coated grids and immunostained with P_0 antibodies and immunogold procedures as described previously (Trapp et al., 1995). Sections were examined in an electron microscope.

EM

Three WT, PLP-null, PLP/P_0-CNS, and P_0-CNS mice were perfused with 2.5% glutaraldehyde, 4% paraformaldehyde, and 0.08 M Sorensen's phosphate buffer at 1, 3, 6, and 12 mo of age. Optic nerves, coronal slices of cerebral cortex, and cervical spinal cords were removed, placed in fixative overnight, osmicated, dehydrated, and processed to Epon 812 as described previously. 1-μm-thick sections were cut on glass knives in an Ultracut Eultramicrotome, mounted on glass slides, stained with toluidine blue, and examined on a light microscope (Axiophot; Carl Zeiss MicroImaging, Inc.).

Transmission EM was performed on select Epon blocks. Sections were cut on a diamond knife, placed on formvar-coated grids, stained with uranyl acetate and lead citrate, and examined in an electron microscope. Optic nerve sections were obtained from all four lines and compared with sciatic nerves from WT mice. The periodicity of compact myelin was determined. The nature and density of axonal ovoids were determined in thin sections from the cerebral cortex blocks of 12-mo-old mice. In addition, the densities of axonal swellings and/or degenerating myelinated fibers in the cortical spinal tract of 6-mo-old mice were compared by *t* test.

X-ray diffraction and myelin structure analysis

Sciatic and optic nerves were dissected from WT and transgenic mice that had been killed by decapitation. During dissection, the tissue was continually rinsed with physiological saline (154 mM NaCl and 5 mM Tris buffer, pH 7.4). Nerves were tied off at both ends with fine silk suture and inserted into medium-containing quartz capillary tubes, which were then sealed at both ends with wax. Diffraction experiments were performed as described previously (Avila et al., 2005) using nickel-filtered, single-mirror-focused CuKα radiation from a fine-line source on a 3.0-kW Rigaku x-ray generator (Rigaku/MSC, Inc.) operated at 40 kV by 16 or 22 mA. The x-ray diffraction patterns for each nerve were recorded first for 10 min (to assess myelin integrity) and then for 2 h using a linear, position-sensitive detector (Molecular Metrology, Inc.). The myelin periodicity was determined from the positions of the peaks (or Bragg orders) in the diffraction patterns, and the membrane profiles (from which the intermembrane spacings at the extracellular and cytoplasmic appositions and membrane bilayer thickness were measured) were calculated by Fourier synthesis from the intensities of the Bragg orders after background subtraction (Avila et al., 2005). The profile shows a periodic fluctuation in electron density through the multilamellar stacking of the myelin membranes. High electron density corresponds to the positions of the lipid polar head groups, and the low density trough corresponds to the centers of the lipid hydrocarbon. The intermediate level of electron density between the membranes indicates protein and water in the spaces at the extracellular and cytoplasmic appositions. Thus, peak-to-peak distances measured off the profiles relate to structural parameters of the membrane structure and its packing.

Nodal density

Density of nodes was quantified in two ways in WT and P_0-CNS optic nerves. Free-floating 30-μm sections of an optic nerve from each of three 1-mo-old WT and P_0-CNS mice were double immunostained as previously described (Yin et al., 2000) using antibodies against Na^+ channels (mouse pan Na^+ channel; Sigma-Aldrich) and caspr (rabbit antibody; a gift from J.A. Trimmer, University of California, Davis,. CA), a paranodal marker. Six nonadjacent areas midway between retinal and chiasmal ends of the optic nerve were imaged using a confocal microscope (TCS-NT; Leica) and software. The fields were collected as a z series of six slices covering 6-μm tissue thickness using 100× (1.3 NA) lens, and nodes were counted within an area 50 × 50 μm in the projected image. Z series projection was necessary for interpretation, as in single slices it was sometimes difficult to unequivocally interpret single spots of staining. Nodal density was also determined by EM. Optic nerves from three WT and three PLP/P_0 mice aged 1 mo were embedded and mounted on Gilder 300 mesh ultrahigh transmission hexagonal grids (hexagonal edges were 43 μm long, and the grid area was 4,800 μm^2). The number of nodes in each of six grid squares was counted per optic nerve.

The authors thank Drs. Ansi Chang and Grahame Kidd for helpful comments and Susan De Stefano for editorial assistance.

This work was supported by National Institutes of Health grants NS38186 and NS38667 (to B.D. Trapp), NS39650 (to D.A. Kirschner), and NS25304 (to W.B. Macklin).

Submitted: 30 September 2005
Accepted: 27 December 2005

References

Arroyo, E.J., Y.T. Xu, L. Zhou, A. Messing, E. Peles, S.Y. Chiu, and S.S. Scherer. 1999. Myelinating schwann cells determine the internodal localization of kv1.1, kv1.2, kvbeta2, and caspr. *J. Neurocytol.* 28:333–347.

Avila, R.L., H. Inouye, R.C. Baek, X. Yin, B.D. Trapp, M.L. Feltri, L. Wrabetz, and D.A. Kirschner. 2005. Structure and stability of internodal myelin in mouse models of hereditary neuropathy. *J. Neuropathol. Exp. Neurol.* 64:976–990.

D'Urso, D., P.J. Brophy, S.M. Staugaitis, C.S. Gillespie, A.B. Frey, J.G. Stempak, and D.R. Colman. 1990. Protein zero of peripheral nerve myelin: biosynthesis, membrane insertion, and evidence for homotypic interaction. *Neuron.* 4:449–460.

Edgar, J.M., M. McLaughlin, D. Yool, S.C. Zhang, J.H. Fowler, P. Montague, J.A. Barrie, M.C. McCulloch, I.D. Duncan, J. Garbern, et al. 2004. Oligodendroglial modulation of fast axonal transport in a mouse model of hereditary spastic paraplegia. *J. Cell Biol.* 166:121–131.

Einheber, S., G. Zanazzi, W. Ching, S. Scherer, T.A. Milner, E. Peles, and J.L. Salzer. 1997. The axonal membrane protein Caspr, a homologue of neurexin IV, is a component of the septate-like paranodal junctions that assemble during myelination. *J. Cell Biol.* 139:1495–1506.

Ferguson, B., M.K. Matyszak, M.M. Esiri, and V.H. Perry. 1997. Axonal damage in acute multiple sclerosis lesions. *Brain.* 120:393–399.

Filbin, M.T., F.S. Walsh, B.D. Trapp, J.A. Pizzey, and G.I. Tennekoon. 1990. The role of myelin P_0 protein as a homophilic adhesion molecule. *Nature.* 344:871–872.

Forghani, R., L. Garofalo, D.R. Foran, H.F. Farhadi, P. Lepage, T.J. Hudson, I. Tretjakoff, P. Valera, and A. Peterson. 2001. A distal upstream enhancer from the myelin basic protein gene regulates expression in myelin-forming schwann cells. *J. Neurosci.* 21:3780–3787.

Garbern, J.Y., D.A. Yool, G.J. Moore, I.B. Wilds, M.W. Faulk, M. Klugmann, K.A. Nave, E.A. Sistermans, M.S. van der Knaap, T.D. Bird, et al. 2002. Patients lacking the major CNS myelin protein, proteolipid protein 1, develop length-dependent axonal degeneration in the absence of demyelination and inflammation. *Brain.* 125:551–561.

Griffiths, I., M. Klugmann, T. Anderson, D. Yool, C. Thomson, M.H. Schwab, A. Schneider, F. Zimmermann, M. McCulloch, N. Nadon, and K.-A. Nave. 1998. Axonal swellings and degeneration in mice lacking the major proteolipid of myelin. *Science.* 280:1610–1613.

Haney, C.A., Z. Sahenk, C. Li, V.P. Lemmon, J. Roder, and B.D. Trapp. 1999. Heterophilic binding of L1 on unmyelinated sensory axons mediates Schwann cell adhesion and is required for axonal survival. *J. Cell Biol.* 146:1173–1183.

Hodes, M.E., and S.R. Dlouhy. 1996. The proteolipid protein gene: double, double, ... and trouble. *Am. J. Hum. Genet.* 59:12–15.

Hudson, L.D. 2004. Proteolipid protein gene. *In* Myelin Biology and Disorders. R.A. Lazzarini, editor. Elsevier Academic Press, San Diego. 401–420.

Kagawa, T., K. Ikenaka, Y. Inoue, S. Kuriyama, T. Tsujii, J. Nakao, K. Nakajima, J. Aruga, H. Okano, and K. Mikoshiba. 1994. Glial cell degeneration and hypomyelination caused by overexpression of myelin proteolipid protein gene. *Neuron.* 13:427–442.

Kidd, G.J., P.E. Hauer, and B.D. Trapp. 1990. Axons modulate myelin protein messenger RNA levels during central nervous system myelination in vivo. *J. Neurosci. Res.* 26:409–418.

Kirschner, D.A., and A.E. Blaurock. 1992. Organization, phylogeneitc variations and dynamic transitions of myelin structure. *In* Myelin: Biology and Chemistry. R.E. Martenson, editor. CRC Press, Boca Raton, FL. 3–78.

Kirschner, D.A., H. Inouye, A.L. Ganser, and V. Mann. 1989. Myelin membrane structure and composition correlated: a phylogenetic study. *J. Neurochem.* 53:1599–1609.

Kirschner, D.A., L. Wrabetz, and M.L. Feltri. 2004. The P0 gene. *In* Myelin Biology and Disorders. R.A. Lazzarini, editor. Elsevier Academic Press, San Diego. 523–545.

Kitagawa, K., M.P. Sinoway, C. Yang, R.M. Gould, and D.R. Colman. 1993. A proteolipid protein gene family: expression in sharks and rays and possible evolution from an ancestral gene encoding a pore-forming polypeptide. *Neuron.* 11:433–448.

Klugmann, M., M.H. Schwab, A. Puhlhofer, A. Schneider, F. Zimmermann, I.R. Griffiths, and K.A. Nave. 1997. Assembly of CNS myelin in the absence of proteolipid protein. *Neuron.* 18:59–70.

Koo, E.H., S.S. Sisodia, D.R. Archer, L.J. Martin, A. Weidemann, K. Beyreuther, P. Fischer, C.L. Masters, and D.L. Price. 1990. Precursor of amyloid protein in Alzheimer disease undergoes fast anterograde axonal transport. *Proc. Natl. Acad. Sci. USA.* 87:1561–1565.

Kurihara, T., M. Sakuma, and T. Gojobori. 1997. Molecular evolution of myelin proteolipid protein. *Biochem. Biophys. Res. Commun.* 237:559–561.

Lappe-Siefke, C., S. Goebbels, M. Gravel, E. Nicksch, J. Lee, P.E. Braun, I.R. Griffiths, and K.A. Nave. 2003. Disruption of Cnp1 uncouples oligodendroglial functions in axonal support and myelination. *Nat. Genet.* 33:366–374.

Lemke, G., and R. Axel. 1985. Isolation and sequence of a cDNA encoding the major structural protein of peripheral myelin. *Cell.* 40:501–508.

Macklin, W.B., C.W. Campagnoni, P.L. Deininger, and M.V. Gardinier. 1987. Structure and expression of the mouse myelin proteolipid gene. *J. Neurosci. Res.* 18:383–394.

Milner, R.J., C. Lai, K.-A. Nave, D. Lenoir, J. Ogata, and J.G. Sutcliffe. 1985. Nucleotide sequences of two mRNAs for rat brain myelin proteolipid protein. *Cell.* 42:931–939.

Nave, K.-A., C. Lai, F. Bloom, and R.J. Milner. 1987. Splice site selection in the proteolipid protein (PLP) gene transcript and primary structure of the DM20 protein of central nervous system myelin. *Proc. Natl. Acad. Sci. USA.* 84:5665–5669.

Norton, W.T., and S.E. Poduslo. 1973. Myelination in rat brain: method of myelin isolation. *J. Neurochem.* 21:749–757.

Pedraza, L., J.K. Huang, and D.R. Colman. 2001. Organizing principles of the axoglial apparatus. *Neuron.* 30:335–344.

Rasband, M.N., E. Peles, J.S. Trimmer, S.R. Levinson, S.E. Lux, and P. Shrager. 1999. Dependence of nodal sodium channel clustering on paranodal axoglial contact in the developing CNS. *J. Neurosci.* 19:7516–7528.

Readhead, C., A. Schneider, I. Griffiths, and K.-A. Nave. 1994. Premature arrest of myelin formation in transgenic mice with increased proteolipid protein gene dosage. *Neuron.* 12:583–595.

Saavedra, R.A., L. Fors, R.H. Aebersold, B. Arden, S. Horvath, J. Sanders, and L. Hood. 1989. The myelin proteins of the shark brain are similar to the myelin proteins of the mammalian peripheral nervous system. *J. Mol. Evol.* 29:149–156.

Scherer, S. 1999. Axonal pathology in demyelinating diseases. *Ann. Neurol.* 45:6–7.

Schmitt, F.O., R.S. Bear, and J.J. Palmer. 1941. X-ray diffraction studies of the nerve myelin sheath. *J. Cell. Comp. Physiol.* 18:31–41.

Seitelberger, F. 1995. Neuropathology and genetics of Pelizaeus-Merzbacher disease. *Brain Pathol.* 5:267–273.

Shapiro, L., J.P. Doyle, P. Hensley, D.R. Colman, and W.A. Hendrickson. 1996. Crystal structure of the extracellular domain from P_0, the major structural protein of peripheral nerve myelin. *Neuron.* 17:435–449.

Stecca, B., C.M. Southwood, A. Gragerov, K.A. Kelley, V.L. Friedrich Jr., and A. Gow. 2000. The evolution of lipophilin genes from invertebrates to tetrapods: DM-20 cannot replace proteolipid protein in CNS myelin. *J. Neurosci.* 20:4002–4010.

Trapp, B.D., and R.H. Quarles. 1984. Immunocytochemical localization of the myelin-associated glycoprotein: fact or artifact? *J. Neuroimmunol.* 6:231–249.

Trapp, B.D., and G.J. Kidd. 2004. Structure of the myelinated axon. *In* Myelin Biology and Disorders. R.A. Lazzarini, editor. Elsevier Academic Press, San Diego. 3–25.

Trapp, B.D., Y. Itoyama, N.H. Sternberger, R.H. Quarles, and H. Webster. 1981. Immunocytochemical localization of P_0 protein in Golgi complex membranes and myelin of developing rat Schwann cells. *J. Cell Biol.* 90:1–6.

Trapp, B.D., P. Hauer, and G. Lemke. 1988. Axonal regulation of myelin protein mRNA levels in actively myelinating Schwann cells. *J. Neurosci.* 8:3515–3521.

Trapp, B.D., G.J. Kidd, P.E. Hauer, E. Mulrenin, C. Haney, and S.B. Andrews. 1995. Polarization of myelinating Schwann cell surface membranes: role of microtubules and the trans-Golgi network. *J. Neurosci.* 15:1797–1807.

Trapp, B.D., A. Nishiyama, D. Cheng, and W. Macklin. 1997. Differentiation and death of premyelinating oligodendrocytes in developing rodent brain. *J. Cell Biol.* 137:459–468.

Trapp, B.D., R.M. Ransohoff, E. Fisher, and R.A. Rudick. 1999. Neurodegeneration in multiple sclerosis: relationship to neurological disability. *Neuroscientist.* 5:48–57.

Waehneldt, T.V. 1990. Phylogeny of myelin proteins. *Ann. NY Acad. Sci.* 605:15–28.

Waehneldt, T.V., J.M. Matthieu, and G. Jeserich. 1986. Appearance of myelin proteins during vertebrate evolution. *Neurochem. Int.* 9:463–474.

Wrabetz, L., M.L. Feltri, A. Quattrini, D. Imperiale, S. Previtali, M. D'antonio, R. Martini, X. Yin, B.D. Trapp, L. Zhou, S.Y. Chiu, and A. Messing. 2000. P_0 glycoprotein overexpression causes congenital hypomyelination of peripheral nerves. *J. Cell Biol.* 148:1021–1034.

Yin, X., T.O. Crawford, J.W. Griffin, P.-H. Tu, V.M.Y. Lee, C. Li, J. Roder, and B.D. Trapp. 1998. Myelin-associated glycoprotein is a myelin signal that modulates the caliber of myelinated axons. *J. Neurosci.* 18:1953–1962.

Yin, X., G.J. Kidd, L. Wrabetz, M.L. Feltri, A. Messing, and B.D. Trapp. 2000. Schwann cell myelination requires timely and precise targeting of P_0 protein. *J. Cell Biol.* 148:1009–1020.

Yoshida, M., and D.R. Colman. 1996. Parallel evolution and coexpression of the proteolipid proteins and protein zero in vertebrate myelin. *Neuron.* 16:1115–1126.